



Deposited via The University of Sheffield.

White Rose Research Online URL for this paper:

<https://eprints.whiterose.ac.uk/id/eprint/97622/>

Version: Accepted Version

Article:

Cseh, L., Mang, X., Zeng, X. et al. (2015) Helically Twisted Chiral Arrays of Gold Nanoparticles Coated with a Cholesterol Mesogen. *Journal of the American Chemical Society*, 137 (40). pp. 12736-12739. ISSN: 0002-7863

<https://doi.org/10.1021/jacs.5b05059>

Reuse

Items deposited in White Rose Research Online are protected by copyright, with all rights reserved unless indicated otherwise. They may be downloaded and/or printed for private study, or other acts as permitted by national copyright laws. The publisher or other rights holders may allow further reproduction and re-use of the full text version. This is indicated by the licence information on the White Rose Research Online record for the item.

Takedown

If you consider content in White Rose Research Online to be in breach of UK law, please notify us by emailing eprints@whiterose.ac.uk including the URL of the record and the reason for the withdrawal request.

Helically twisted chiral arrays of gold nanoparticles coated with a cholesterol mesogen

Liliana Cseh^{#,†}, Xiaobin Mang[♦], Xiangbing Zeng[♦], Feng Liu^{♥,♦}, Georg H. Mehl^{##}, Goran Ungar^{*,♦,*}, Giuliano Siligardi[▲]

[#]Department of Chemistry, University of Hull, Hull HU6 7RX, UK

^{*}Department of Physics, Zhejiang Sci-Tech University, Hangzhou 310018, China

[♦]Department of Materials Science and Engineering, University of Sheffield, Sheffield S1 3JD, UK

[♥]State Key Laboratory for Mechanical Behavior of Materials, Xi'an Jiaotong University, Xi'an, 710049, P. R. China.

[▲]Diamond Light Source, Harwell, Didcot OX11 0DE, UK

KEYWORDS. *metal, nanoparticle, liquid crystal, chiral, helix, circular dichroism, GISAXS*

Gold nanoparticles have been prepared, surface-functionalized with a 1:1 molar mixture of a hexylthiol ligand and a chiral mesogenic ligand consisting of a cholesterylbenzoate attached via an undecylthiol spacer. Grazing incidence X-ray diffraction showed that, upon annealing, a columnar liquid crystal (LC) structure develops, with the nanoparticles forming strings on a regular oblique 2d lattice. Synchrotron radiation circular dichroism is substantially enhanced upon the isotropic-LC transition. In the proposed structural model, layers of gold columns rotate by a small angle relative to their neighbors, the columns winding around a helical axis. The work demonstrates that it is possible to obtain chiral LC superstructures from nanoparticles coated with chiral mesogen without the addition of a separate liquid crystal or chiral dopants. The results provide direction in the development of plasmonic metamaterials interacting selectively with circularly polarized light.

The breaking of symmetry is one of the most basic tools to introduce functionality into organic materials. In many nematic liquid crystal (LC) display applications the addition of a small amount of a chiral additive is critical for their performance. The specific optical properties of chiral nematics are also used in nature, striking examples being the chiral nematic photonic structures in the shells of beetles.^{1,2} A number of methods have been designed to arrange nanoparticles (NPs) in chiral assemblies.^{3,4,5,6,7} The amplification of optical effects by the inclusion of metallic NPs in chiral nematic LCs has recently been explored very actively, especially as the chiral organization of gold or silver NPs promises fascinating metamaterial behaviour.^{8,9,10,11} Optical metamaterials capable of interacting with circularly polarized (CP) light, based on helical structures, are of considerable interest as CP light can be used e.g. in optical communications between spin-LEDs,¹² in displays,¹³ or in quantum-based optical computing.¹⁴ So far efforts to obtain chiral nematics filled with NPs have either relied on adding hydrocarbon group-capped NPs to a chiral nematic matrix or, alternatively, on functionalizing gold NPs with chiral groups and dispersing them in a nematic liquid crystal.^{15,16,17,18,19,20,21,22} In the main it has been found that NPs aggregate in the defects of the LC texture. This is possibly mediated by the pinning of features of defects such as fingerprint or schlieren textures to surfaces, providing thus a means of

spatial NP assembly. However, this method requires a very careful control of the NP concentration in order to avoid phase separation and precipitation. To the best of our knowledge there have been so far no reported investigations of functionalized NPs *per se* forming a chiral LC phase. We note that, in order to achieve significant plasmonic effects that could potentially lead to useful photonic metamaterials, a relatively high density of metallic NPs is required that is unlikely to be obtainable by NP doping of LCs.^{10,16}

Thus we report here the synthesis and investigation of the phase behaviour of a LC-NP system, which is intrinsically chiral. Cholesterol-based mesogens are attached to the surface of gold NPs via alkylthiol spacers. The formation of an ordered superlattice is studied by a combination of X-ray diffraction and circular dichroism (CD), both techniques using mainly synchrotron radiation (hereafter SRCD denotes experiments using synchrotron light source). The structural model is proposed based on an oblique columnar phase made up of strings of gold NPs, each layer of columns slightly twisted relative to the neighboring layers. We believe that the result reported herein will help create plasmonic metamaterials selectively interacting with circularly polarized light.

The synthesis and chemical characterization of the cholesterol-based thiol ligand **1** is described in the Supporting

Information (SI). The synthesis of LC functionalized LC-NPs follows essentially the route described earlier.^{23,24} Hexylthiol NPs are synthesized according to a Brust-Schiffrin approach, and an exchange reaction introduced a cholesteryl group attached end-on to a thioalkyl chain (see Chart as the mesogenic unit). Following purification using size exclusion chromatography over biobeads, gold NPs were obtained, coated with a 1:1 mixture of n-hexylthiol and mesogens **1**, denoted **AuCholC6**.

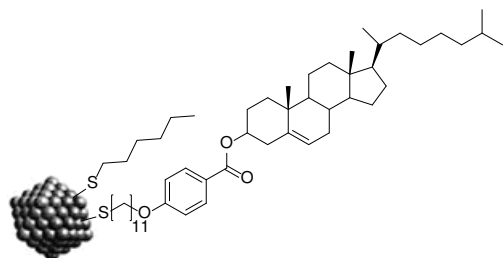


Chart 1.
Sketch of functionalized gold nanoparticle AuCholC6; total number of organic ligands 78 ± 5 of which 37 ± 5 are cholesteryl based mesogens

From thermogravimetric scanning (Figure S3) the weight fraction of gold in **AuCholC6** was determined to be 39%. From elemental analysis the molar fractions of hexylthiol and mesogenic ligands were determined as 47% and 53% of the organic coating of the NPs (see SI, Section 1.4). This ratio was also confirmed by NMR. A transmission electron micrograph (TEM) of **AuCholC6** precipitated from dilute solution is shown in Figure 1a. The average particle diameter from TEM is 1.7 ± 0.4 nm. Based on these data we obtain the average number of Au atoms per particle as 151, and a total number of ligands per particle as 78 ± 5 , 37 ± 5 of which are mesogens. This is in accord with earlier work^{25,26} and supported by recent results measuring ligand densities of up to ~ 6.3 ligands/nm². Together with a surface area of the NPs estimated to be 11.5 to 13 nm² (ref. 25), this gives 73-82 ligands per particle.²⁷

Based on DSC and polarized optical microscopy (POM) the phase sequences obtained for **1** and **AuCholC6** are listed in Table 1. Polarized optical micrographs of the chiral nematic (cholesteric) phase N* and the twist grain boundary (TGB) phase of **1** are shown in Figure S4 of SI, and X-ray patterns in Figure S7.

Table 1. Transition temperatures and enthalpies as determined by DSC

Compd	T_i / °C (Enthalpies J/g)
1	Cr 114.2 (43.50) SmA* 132.6 N* 186.3 (0.42) Iso or Cr 114.2 TGB 132.61 N* 186.3 Iso (see Figure S4)
AuCholC6	Cr 58.2 X 160 Iso and slow dec.

N* = chiral nematic, SmA* = chiral smectic A; X = unknown mesophase (twisted oblique columnar LC, as determined from GISAXS and CD, see below); Iso = isotropic liquid.

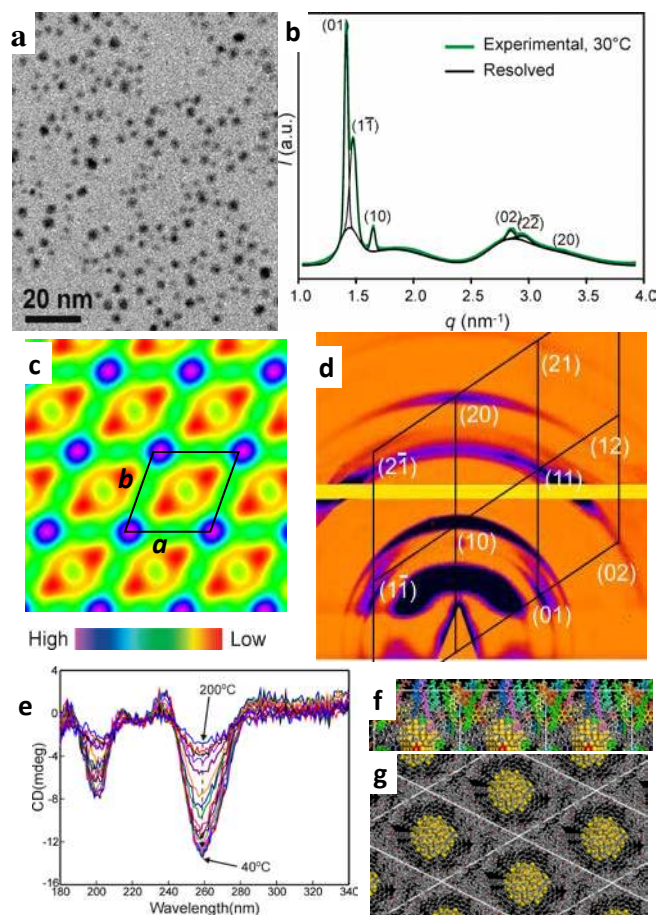


Figure 1 (a) TEM picture of **AuCholC6** on carbon surface. (b) Powder SAXS curve of annealed **AuCholC6** recorded at 30°C; resolved components are superimposed and indexed. (c) ED map perpendicular to the columns based on intensities of the six reflections in (b); all phase angles are 0. (d) GISAXS pattern of a slowly cooled thin film of **AuCholC6** in the mesophase; the reciprocal net is superimposed giving the Miller indices. (e) CD spectra of a thin film of **AuCholC6** recorded every 10 degrees upon cooling from the isotropic liquid (200°C) to 40°C; note the largest increase in ellipticity between 160 °C and 150 °C, coinciding with the isotropic – columnar transition observed by X-ray diffraction (see also Figure S17); (f) side and (g) top views of a model of several unit cells of **AuCholC6** after molecular dynamics annealing, with unit cell parameters as determined by experiment; in (f) each mesogen is colored differently for clarity.

Powder small angle X-ray scattering (SAXS) on annealed **AuCholC6** revealed a mesophase (X in Table 1) with long-range positional order, stable up to 90 °C – Figure 1b (also Figure S6). Grazing incidence small angle X-ray scattering (GISAXS) experiments were also performed on thin films to obtain oriented samples which helped index the Bragg reflections. For this purpose a film was melt-cast on silicon substrate and then cooled from 130 to 30 °C at 0.2 °C/min under vacuum. The Bragg spacings in the GISAXS pattern (Figure 1d) match well those in the powder pattern (see also comment on the diffuse scatter in section 4 of SI). The Bragg reflections were indexed on an oblique 2D lattice (Figure 1d) with unit cell parameters $a = 4.54$ nm, $b = 5.28$ nm and the angle $\gamma = 57.0^\circ$. The

measured and calculated d -spacings and diffraction intensities are given in Table S1.

The position of the diffuse maximum next to (10) observed in the powder pattern corresponds to a d -spacing of 3.7 nm if Bragg equation were used; however in dense disordered particle systems the correlation function maximum is usually asymmetric²⁸ and as a guide ca. 10% should be added to the “Bragg” value when estimating the average particle distance, giving thus a value of ca. 4.1 nm. This is likely to correspond to the average gold NP distance along the columns.

An electron density (ED) map of the columnar mesophase was reconstructed using the diffraction intensities from the powder pattern in Figure 1b (see also Figure S9 and numerical data in Table S1). The ED map in Figure 1c is a projection of the 3D map onto the xy plane. The purple-blue high ED regions are the projections of the gold NP strings, surrounded by the low density organic ligands. This map is unusual compared to those obtained previously in systems where the NPs were coated with non-chiral mesogens^{29, 30, 31} in that the columnar phase is oblique rather than hexagonal or rectangular (see below).

Table S2 details the calculation of the average Au NP diameter based on the above unit cell parameters, the gold weight fraction from TGA, and the assumption that there is one NP per unit cell. The Au NP diameter obtained is 1.69 nm, in excellent, somewhat coincidental, agreement with the value of 1.7 nm obtained from TEM.

In order to establish whether there is helical order in the mesophase of **AuCholC6** we recorded CD spectra as a function of temperature. If the mesophase contained helical twist, an enhancement of the CD signal would occur upon the isotropic–mesophase transition. Fortunately, the LC domains were very small and numerous (see Figure S5), causing most of the interfering ellipticity due to linear dichroism and birefringence within the illuminated area to cancel.^{32, 33} That these interfering effects were indeed negligible was ascertained by rotating the sample during the recording; angular dependence of CD spectrum of **AuCholC6** is shown in Figure S16. Sample rotation, xy scanning, recording at high temperatures and prevention of gravity-induced flow were all made possible by the use of the bright, vertically deflected light beam of synchrotron radiation (see S115) only available at module A of B23 beamline.³⁴ The temperature series of SRCD spectra is shown in Figure 1e. The increasing CD in the UV bands at 200 and 260 nm with lowering temperature is clearly evident. The largest jump is seen between 160°C and 150°C, i.e. at the isotropic–mesophase transition temperature. The temperature-dependent intensity of the 260 nm CD band is plotted in Figure S17, showing typical weak first-order phase transition features. This behaviour together with the fact that for the film the CD at about 260 nm (Fig. 1e) has opposite sign than that in solution (Fig. S20) is a strong indication of the existence of helical twist in the mesophase superstructure.

The question to be addressed is how is it possible to reconcile helical twist with a 2D-ordered columnar LC structure? There have been numerous reported examples of intracolumnar helical order in thermotropic^{35, 36, 37} columnar systems – see e.g. review ref. 38. But these examples have all involved “classical” column-forming mesogens, typically disc-like or wedge-like with spread-out flexible tails forming a shield around each column. In contrast, the ligand in **AuCholC6** is a typical nematogen, albeit chiral, with a tendency to align nearly parallel to its neighbours and form a cholesteric phase. Furthermore, the fact that the 2D lattice is oblique does not support intracolumnar helical structure. Instead, we propose a model based on the cholesteric arrangement of the mesogens but with strings of gold NPs threaded through it – see sketch in Figure 2. In this model the layers of gold columns rotate by a small angle relative to their neighbors, the columns winding around the vertical axis forming a helix. As the POM textures were too fine and did not show a discernible fingerprint pattern characteristic of the cholesteric LC phase, we could not determine the pitch of the helix. No selective reflection of light was observed, hence the pitch is likely to be outside the visible light wavelengths. The departure from hexagonal symmetry is consistent with this model. Notably, as would be expected, the twist plane (horizontal in Figure 1c) is the most densely packed plane with the shortest intercolumnar distance within the plane.

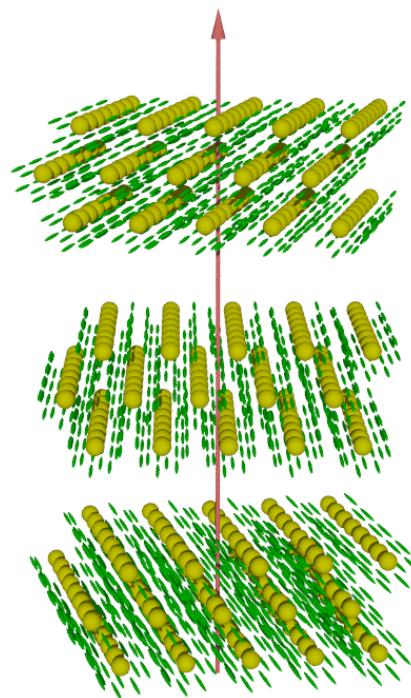


Figure 2. Schematic representation of the chiral columnar LC phase of **AuCholC6**. Yellow: gold NPs, green: mesogenic cholesteryl ligands. The breaks in the stacks of columnar layers indicate that the helical pitch is long on the molecular scale.

In Figure 2 the cholesterol mesogens are drawn with their axis broadly parallel to the NP columns, as has been observed for other rod-shaped mesogens attached to

NPs,^{28,29} an arrangement driven by the nematogenic tendency of the cholesteryl benzoate and mediated by the long flexible spacer. The structure is supported by molecular modelling – Figures 1f,g. See also Figures S12 and S13, the former showing an energy-minimized conformation of the mesogenic ligand. The number of gold atoms and mesogenic ligands per cell are also as determined by experiment (see above). The alternative models in which the cholesteric mesogens would lie preferentially in planes perpendicular to NP column axis would require a larger intercolumnar distance (larger cell cross-section) and a considerably smaller intracolumnar NP spacing, hence are judged less likely. Additional support for the model is presented in Section 3 of SI.

It is stressed that the sketch in Figure 2 does not imply a discontinuous twist and that the breaks are meant only to illustrate the presumed large size of the helical pitch compared to the molecular scale.

In summary, we have demonstrated that it is possible to obtain chiral LC superstructures from undiluted NPs coated with chiral mesogens. The high NP content achievable in this way should allow the production of plasmonic metamaterials interacting selectively with CP light, extending the range of potential optical applications of LC-NP systems. In future work we will attempt to include mesogens with stronger chirality in order to shorten the helical pitch, and to increase the NP size in order to enhance the plasmonic response.

ASSOCIATED CONTENT

Supporting Information. Synthesis and chemical characterization; instrumental methods; optical microscopy; X-ray diffraction – additional data; molecular models, UV and Vis spectra. This material is available free of charge via the Internet at <http://pubs.acs.org>.

AUTHOR INFORMATION

Corresponding Author

* g.ungar@sheffield.ac.uk; *g.h.mehl@hull.ac.uk

Present Addresses

†Institute of Chemistry Timisoara of Romanian Academy, Timisoara - 300223, lili_cseh@yahoo.com

Author Contributions

All authors have given approval to the final version of the manuscript.

Funding Sources

Financial support is acknowledged for the joint NSF-EPSRC project (EPSRC EP/K034308), the Leverhulme Foundation (RPG-2012-804), for GU, the “1000 Talents” program of the Government of China and for LC through the EPSRC project EP/D058066 and the EU FP7 project 228455 “Nanogold”.

ACKNOWLEDGMENT

For help with X-ray and CD synchrotron experiments we thank Drs. G. Nisbet and Prof. S. Collins of beamline I16, Prof. N. Terrill of I22 and Dr. Tamas Javorfi of B23 at Diamond Light Source.

REFERENCES

- 1 Neville, A. C.; Caveney S. *Biol. Rev.* **1969**, *44*, 531.
- 2 Sharma V.; Crne M.; Park J. O.; Srinivasarao M. *Science*, **2009**, *325*, 449.
- 3 Pendry, P. B. *Science*, **2004**, *306*, 1353.
- 4 Valev V. K.; Baumberg J. J.; Sibila C.; Verbiest T. *Adv. Mater.* **2013**, *25*, 2517.
- 5 Rodrigues S. P.; Lan S.; Kang L.; Cui Y.; Cai W. *Adv. Mater.* **2014**, *26*, 6157.
- 6 Xia Y.; Zhou Y.; Tang Z. *Nanoscale*, **2011**, *3*, 1374.
- 7 Ma W.; Kuang H.; Xu L.; Chang W. S.; Zhang H.; Sun M.; Zhu Y.; Zhou Y.; Liu L.; Xu C.; Link S.; Kotov N. A. *Sci. Rep.* **2013**, *3*, 1934.
- 8 Lilly G. D.; Agarwal A.; Srivastava S.; Kotov A. N. *Small*, **2011**, *7*, 2004.
- 9 Bierman M. J.; Lau Y. K. A.; Kvit A. V.; Schmitt A. L.; Jin S. *Science*, **2008**, *320*, 1060.
- 10 Rockstuhl C.; Lederer F.; Etrich C.; Pertsch T.; Scharf T. *Phys. Rev. Lett.* **2007**, *99*, 017401.
- 11 Gautier, C.; Bürgi, T. *J. Am. Chem. Soc.* **2006**, *128*, 11079.
- 12 Farshchi, R.; Ramsteiner, M.; Herfort, J.; Tahraoui, A.; Grahn, H. T. *Appl Phys Lett.* **2011**, *98*, 162508.
- 13 Singh, R. *et al. Optical Materials* **2012**, *34*, 716.
- 14 Sherson, J. F.; Krauter, H.; Olsson, R. K.; Julsgaard, B.; Hammerer, K.; Cirac, I.; Polzik, E. S. *Nature* **2006**, *443*, 557.
- 15 Mitov, M.; Portet, C.; Bourgerette, C.; Snoeck, E.; Verelst, M. *Nature Mat.* **2002**, *1*, 229.
- 16 Mitov, M.; Bourgerette, C.; de Guerville, F. *J. Phys.: Condens. Matter* **2004**, *16*, S1981.
- 17 Qi, H.; O’Neil, J.; Hegmann, T. *J. Mater. Chem.* **2008**, *18*, 374.
- 18 Qi, H.; Hegmann, T. *J. Amer. Chem. Soc.* **2008**, *130*, 14201.
- 19 Ayebe, H.; Grand, J.; Truong, S.; Aubard, J.; Felidj, N.; Mlayah, A.; Lacaze, E. *J. Mater. Chem.* **2012**, *22*, 7856.
- 20 Sharma, A.; Mori, T.; Lee, H.-C.; Worden, M.; Bidwell, E.; Hegmann, T. *ACS Nano* **2014**, *8*, 11966.
- 21 Pendry, J.S.; Merchiers, O.; Coursault, D.; Grand, J.; Ayebe, H.; Greget, R.; Donnio, B.; Gallani, J.L.; Rosenblatt, C.; Felidj, N.; Borensztein, Y.; Lacaze, E.; *Soft Matter*, **2013**, *9*, 9366.
- 22 Choudhary, A.; Singh, G.; Biradar, A.M.; *Nanoscale*, **2014**, *6*, 7743.
- 23 Cseh, L.; Mehl, G.H. *J. Am. Chem. Soc.* **2006**, *128*, 13377.
- 24 Dintinger, J.; Tang, B. J.; Zeng, X.; Liu, F.; Kienzler, T.; Mehl, G. H.; Ungar, G.; Rockstuhl, C.; Scharf, T. *Adv. Mater.* **2013**, *25*, 1999.
- 25 Hostetler, M. J.; Wingate, J. E.; Zhong, C.-J.; Harris, J. E.; Vachet, R. W.; Clark, M. R.; Londono, J. D.; Green, S. J.; Stokes, J. J.; Wignall, G. D.; Glish, G. L.; Porter, M. D.; Evans, N. D.; Murray, R. W. *Langmuir* **1998**, *14*, 17-30.
- 26 Labande, A.; Ruiz, J.; Astruc, D.; *J. Am. Soc.* **2002**, *124*, 1782-1789; Ruiz, M.C.J.; Blais, J.C.; Astruc; *D J. Am. Chem. Soc.* **2003**, *125*, 2017-2628.
- 27 Hinterwirth, H.; Kappel, S.; Waitz, T.; Prohaska, T.; Lindner, W.; Lämmerhofer, M.; *ACS Nano*, **2013**, *7*, 1129-1136
- 28 Schulz, G. V. *Z. Phys. Chem. B-Chem. Elem. Aufbau. Mater.* **1939**, *43*, 25.
- 29 Zeng, X. B.; Liu, F.; Fowler, A.G.; Ungar, G.; Cseh, L.; Mehl, G. H.; Macdonald, J. E. *Adv. Mater.* **2009**, *21*, 1746.

³⁰ Mang, X.; Zeng, X. B.; Tang, B.; Liu, F.; Ungar, G.; Zhang, R.; Cseh, L.; Mehl, G. H. *J. Mater. Chem.* **2012**, *22*, 11101.

³¹ Kanie, K.; Matsubara, M.; Zeng, X. B.; Liu, F.; Ungar, G.; Nakamura, H.; Muramatsu, A. *J. Am. Chem. Soc.*, **2012**, *134*, 808.

³² Gottarelli, G.; Lena, S.; Masiero, S.; Pieraccini, S.; Spada, G. *P. Chirality*, **2008**, *20*, 471.

³³ Otani, T.; Araoka, F.; Ishikawa, K.; Takezoe, H. *J. Am. Chem. Soc.* **2009**, *131*, 12368).

³⁴ Siligardi, G.; Hussain, R.; in *Structural Proteomics: High-Throughput Methods*, Methods in Molecular Biology, Owens, R. J (ed) *Structural Proteomics: High-Throughput Methods*, Methods in Molecular Biology, **2015**, *126*, 255-276.

³⁵ Fontes, E.; Heiney, P.A.; de Jeu, W.H. *Phys. Rev. Lett.* **1988**, *61*, 1202.

³⁶ Malthéte, J.; Collet, A. *J. Am. Chem. Soc.* **1987**, *109*, 7544.

³⁷ Shcherbina, M. A.; Zeng, X. B.; Tadjiev, T.; Ungar, G.; Eichorn, S. H.; Phillips, K. E. S.; Katz, T. J. *Angew. Chem. Int. Ed.* **2009**, *48*, 7837.

³⁸ Vera, F.; Serrano, J. L.; Sierra, T. *Chem. Soc. Rev.* **2009**, *38*, 781.

Insert Table of Contents artwork here

